The Astrophysical Journal, 927:159 (10pp), 2022 March 10 https://doi.org/10.3847/1538-4357/ac4af4

Toward a Realistic Evaluation of Transport Coefficients in Non-equilibrium Space Plasmas

Edin Husidic[1,2], Klaus Scherer[3,4], Marian Lazar[1,3], Horst Fichtner[3,4], and Stefaan Poedts[1,5]
[1] Centre for mathematical Plasma Astrophysics, Department of Mathematics, KU Leuven, Celestijnenlaan 200B, 3001 Leuven, Belgium; edin.husidic@kuleuven.be
[2] Department of Physics and Astronomy, University of Turku, 20014 Turku, Finland
[3] Institut für Theoretische Physik, Lehrstuhl IV: Plasma-Astroteilchenphysik, Ruhr-Universität Bochum, D-44780 Bochum, Germany
[4] Research Department, Plasmas with Complex Interactions, Ruhr-Universität Bochum, D-44780 Bochum, Germany
[5] Institute of Physics, University of Maria Curie-Skłodowska, Pl. M. Curie-Skłodowska 5, 20-031 Lublin, Poland
Received 2021 December 3; revised 2022 January 5; accepted 2022 January 11; published 2022 March 11

Abstract

Recent studies have outlined the interest for the evaluation of transport coefficients in space plasmas, where the observed velocity distributions of plasma particles are conditioned not only by the binary collisions, e.g., at low energies, but also by the energization of particles from their interaction with wave turbulence and fluctuations, generating the suprathermal kappa-distributed populations. This paper provides a first estimate of the main transport coefficients based on regularized kappa distributions, which, unlike standard kappa distributions (SKDs), enable macroscopic parameterization without mathematical divergences or physical inconsistencies. All transport coefficients derived here, i.e., the diffusion and mobility coefficients, electric conductivity, thermoelectric coefficient, and thermal conductivity, are finite and well defined for all values of $\kappa > 0$. Moreover, for low values of κ (i.e., below the SKD poles), the transport coefficients can be orders of magnitudes higher than the corresponding Maxwellian limits, meaning that significant underestimations can be made if suprathermal electrons are ignored.

Unified Astronomy Thesaurus concepts: Space plasmas (1544); Plasma astrophysics (1261); Collision processes (2065); Solar wind (1534); Heliosphere (711); Astrophysical processes (104)

1. Introduction

Plasma is by far the most dominant state of perceivable matter in the universe. Due to the opportunity of in situ measurements, the heliosphere is a plasma system of the highest interest. The solar wind is emitted from the Sun as a continuous stream of electrons and protons, and fills the heliospheric bubble (Marsch 2006; Verscharen et al. 2019). The high energy, as well as the dilute nature of space plasmas, points toward a reduced influence of binary collisions, so that there is no full relaxation to the thermal equilibrium, characterized by Maxwellian distributions (Pierrard & Lazar 2010). Indeed, observations show nonthermal velocity distributions maintained for long periods (Maksimovic et al. 2005; Zouganelis et al. 2005), most probably due to the interaction of particles with fluctuations (Vocks & Mann 2003; Marsch 2006; Vocks et al. 2008). While wave-particle interactions occur at all heliocentric distances and their effects become more relevant at larger distances (>1 au), it is argued that Coulomb collisions between particles can still play a significant role toward lower distances from the Sun, i.e., lower than 1 au (Salem et al. 2003; Landi et al. 2010, 2012). Indeed, solar wind models using a purely exospheric approach, i.e., a collision-less model, fail to accurately reproduce the global expansion of the solar wind observed in situ, and are, at best, helpful approximations to gain insight into basic energetic processes (see the reviews by Marsch 1994 and Echim et al. 2011). Thus, to realistically account for processes like dissipation, diffusion, and viscosity, these models must also accommodate particle-particle collisions, or at least incorporate their effects, e.g., for low-energy populations (with high so-called collisional age; Bourouaine et al. 2011).

Space probes regularly observe nonthermal plasma particle velocity distributions with enhanced suprathermal tails, well described by the family of kappa (or κ-power law) distributions (Pierrard & Lazar 2010; Scherer et al. 2020; Lazar & Fichtner 2021). Kappa distributions are the result of such combined effects, both of particle-particle collisions conditioning a quasi-Maxwellian profile at low energies, and of particle interactions with wave turbulence and fluctuations, which can explain the suprathermal tails of these distributions (Vocks & Mann 2003; Yoon 2014). The transport theory for such plasma populations must therefore rely on a kinetic approach centered on the Boltzmann transport equation (BTE) that describes the time/space evolution of particle velocity distribution. Alternatively, plasma transport theory provides a simpler, macroscopic approach to account for the moments of the velocity distributions and their variations, namely by relating fluxes (e.g., heat flux or electric currents) to their sources (e.g., electromagnetic fields, gradients of temperature, or density), through linear relationships. Coefficients of proportionality are termed transport coefficients and may determine the transport of mass, momentum, and energy. (Braginskii 1965; Balescu 1988; Dum 1990). The mathematical formalism for the transport approach used in the present work (including the simplified ansatz to allow for analytical or numerical computation of the collision integral) is presented in Section 2.

Recently, the electric conductivity, the thermoelectric coefficient, the thermal conductivity, and the diffusion and mobility coefficients have been derived and estimated for electron populations described by the standard kappa distribution (SKDs; Husidic et al. 2021). Introduced in the pioneering works of Olbert (1968) and Vasyliūnas (1968), these original SKD models have the merit of allowing a direct and straightforward comparison with the quasi-thermal population at the low-energy core of kappa distribution, reproduced in this case by the Maxwellian limit

($\kappa \to \infty$) (Lazar et al. 2015, 2016). Such a comparison can thus emphasize the contribution of suprathermal populations to any property of the plasma system. Husidic et al. (2021) have shown that all the aforementioned transport coefficients are systematically and markedly enhanced in the presence of suprathermal electrons. Other similar studies attempting to evaluate these coefficients for SKD electrons (Ebne Abbasi et al. 2017; Wang & Du 2017; Guo & Du 2019) have in general adopted variants of kappa distributions, which provide only underestimates of transport coefficients (Husidic et al. 2021).

However, even in the original forms, the SKDs themselves have a number of well-known limitations. Namely, SKDs do allow for finite (convergent) macroscopic velocity moments M_l of order l only if power-law exponents are sufficiently high, i.e., $\kappa > (l+1)/2$. These limitations have been resolved by defining the regularized kappa distributions (RKDs; Scherer et al. 2017); see also Appendix A. Moreover, the RKDs exhibit exponential cutoffs of the suprathermal tails, able to minimize the unphysical implication of superluminal particles with speeds exceeding the speed of light in vacuum (Scherer et al. 2019).

In the present paper, we compute the main transport coefficients for the electrons for the first time described by the RKDs (Section 2), namely the diffusion coefficient (Section 2.1), the mobility coefficient (Section 2.2), the electric conductivity (Section 2.3), the thermoelectric coefficient (Section 2.4), and the thermal conductivity (Section 2.5). The transport coefficients are well defined, taking finite values for any value of the power exponent $\kappa > 0$, and are not affected by any limitation given by the singularities of SKDs, e.g., for low values of $\kappa \leqslant (l+1)/2$ (Lazar et al. 2020). Conclusions and an outlook for potential future work are formulated in Section 3. In the appendix, we briefly discuss the RKD (Appendix A), and give useful formulas and solutions of the integrals (Appendix B) occurring in Section 2. Furthermore, in Appendix C, we present approximations that extend the scope of transport coefficients even to $\kappa \to 0$, and tabulated in Table 1 the expressions obtained for the transport coefficients for a suggestive comparison on different distribution functions.

2. Transport Coefficients

Within transport theory, we may start from the velocity moments of the BTE and use macroscopic laws for the electric field, the electric current density, the heat flux, and the particle flux. Comparisons between the moment equations and macroscopic laws allow us to identify the transport coefficients and to derive their expressions. In order to study the effects of suprathermal particles on the transport coefficients, we assume heavy and stationary ions and mobile electrons described by the RKD.

The macroscopic relationships between fluxes and their sources used in the present work are

$$\boldsymbol{\Gamma} = -D\,\nabla n - \mu\, n\, \boldsymbol{E}, \tag{1}$$

$$\boldsymbol{\Gamma} = \langle \boldsymbol{v} \rangle = \int d^3v\, \boldsymbol{v}\, f, \tag{2}$$

$$\boldsymbol{E} = \frac{1}{\sigma}\boldsymbol{j} + \alpha\, \nabla T, \tag{3}$$

$$\boldsymbol{j} = q \int d^3v\, \boldsymbol{v}\, f, \tag{4}$$

$$\boldsymbol{q} = (\phi + \alpha\, T)\boldsymbol{j} - \lambda\, \nabla T, \tag{5}$$

$$\boldsymbol{q} = \frac{1}{2} m \int d^3v\, v^2\, \boldsymbol{v}\, f = \int d^3v\, \varepsilon\, \boldsymbol{v}\, f. \tag{6}$$

The particle flux density $\boldsymbol{\Gamma}$, defined as the average of velocity $\boldsymbol{v}$ (Equation (2)), can occur due to a gradient in number density n or the presence of an electric field $\boldsymbol{E}$ in an extended Fick's law in Equation (1). The corresponding transport coefficients are the diffusion coefficient D and the mobility coefficient μ, respectively. Equation (3) is a generalized Ohm's law and sets the electric field in relation to electric current density $\boldsymbol{j}$, defined in Equation (4) with electric charge q, and gradient in temperature T. There, the related transport coefficients are the electric conductivity σ and the thermoelectric coefficient α, respectively. The heat flux $\boldsymbol{q}$ as defined in Equation (6) can arise due to an electric current density or a temperature gradient, expressed through an extended Fourier's law in Equation (5), where λ is the thermal conductivity, ϕ is the electric potential related to the electric field via $\boldsymbol{E} = -\nabla\phi$, and α is the same thermoelectric coefficient as in Equation (3). More details can be found in Spatschek (1990), Boyd & Sanderson (2003), and Goedbloed et al. (2019).

The evolution of a distribution function f in time and space is given by the partial differential equation

$$\frac{\partial f}{\partial t} + \boldsymbol{v}\cdot\nabla f + \frac{q}{m}\left[\boldsymbol{E} + \frac{1}{c}(\boldsymbol{v}\times\boldsymbol{B})\right]\cdot\nabla_{\boldsymbol{v}} f = \mathcal{C}(f), \tag{7}$$

which is called the BTE. Here, we assume that the electric and magnetic fields $\boldsymbol{E}$ and $\boldsymbol{B}$ contain both the imposed and self-generated fields. While ∇ is the standard spatial derivative, $\nabla_{\boldsymbol{v}}$ expresses the velocity gradient. The collision term is denoted by $\mathcal{C}(f)$. Assuming stationary transport and neglecting the magnetic field in Equation (7), we find

$$\boldsymbol{v}\cdot\nabla f - \frac{q}{m}\boldsymbol{E}\cdot\nabla_{\boldsymbol{v}} f = \mathcal{C}(f). \tag{f8}$$

Collisions between particles cause changes in the velocity distribution. Assuming that the changes are relatively small, we can linearize the distribution function and write it as a sum of the stationary solution f_0 and a small perturbation f_1, which yields

$$f(\boldsymbol{r}, \boldsymbol{v}, t) = f_0(\boldsymbol{r}, \boldsymbol{v}) + f_1(\boldsymbol{r}, \boldsymbol{v}, t). \tag{9}$$

The collision term in the BTE is in its most general form an integral that proves to be very challenging to exactly compute. To overcome this issue, we use a Krook-type collisional operator (Bhatnagar et al. 1954) for $\mathcal{C}(f)$, given by

$$\mathcal{C}(f) = -\nu_{\rm ei}(v)(f - f_0) = -\nu_{\rm ei}(v) f_1. \tag{10}$$

This ansatz assumes that the perturbed distribution function f relaxes toward the stationary solution f_0 under the effect of collisions that occur with frequency $\nu_{\rm ei}(v)$ as a function of speed v. Here, the subscript "ei" indicates that collisions occur only between electrons and stationary ions. For $\nu_{\rm ei}(v)$, we used the expression given by Helander & Sigmar (2005):

$$\nu_{\rm ei}(v) = \nu_{\rm ei} = \frac{4\,\pi\, n_{\rm e}\, z\, e^4\, L^{\rm ei}}{m_{\rm r}\, m_{\rm e}\, v^3} \approx \frac{4\,\pi\, n_{\rm e}\, z\, e^4\, L^{\rm ei}}{m_{\rm e}^2\, v^3} \tag{11}$$

with electron number density $n_{\rm e}$, ion charge number z, elementary charge e, electron mass $m_{\rm e}$, and reduced mass $m_{\rm r} \equiv m_{\rm e}\, m_{\rm i}/(m_{\rm e} + m_{\rm i}) \simeq m_{\rm e}$ (with ion mass $m_{\rm i}$), and Coulomb logarithm $L^{\rm ei} = \ln\Lambda$, where Λ is the (normalized) electron Debye length. In the following, we omit the subscript e in n and

m as they always refer to electrons for the remaining part. We further note that considering only collisions between electrons and ions is a generic choice, relevant enough for low heliocentric distances, e.g., in the outer corona where $T_e < T_i$ is observed (Landi 2007; Landi & Cranmer 2009), while for larger distances, where $T_e \sim T_i$, electron–electron collisions with frequency $\nu_{ee} \gtrsim \nu_{ei}$ must also be taken into account.

By inserting the linearized distribution function from Equation (9) into the simplified BTE from Equation (8), we obtain

$$\boldsymbol{v} \cdot \nabla f_{\mathrm{RKD}} - \frac{e}{m}\boldsymbol{E} \cdot \nabla_v f_{\mathrm{RKD}} = -\nu_{ei} f_1, \tag{12}$$

where we set f_0 to the RKD f_{RKD} and neglected all second-order terms of the spatial and velocity gradients of perturbation f_1. For the derivation of the transport coefficients, we did not use the RKD in its original representation displayed in Equation (A1), but rewrote it in terms of kinetic energy $\varepsilon = m\,v^2/2$ and corresponding Maxwellian temperature T to

$$f_{\mathrm{RKD}} = N_{\mathrm{RKD}}\left(1 + \frac{\varepsilon}{\kappa\, k_B\, T}\right)^{-(\kappa+1)} \exp\left(-\xi^2 \frac{\varepsilon}{k_B\, T}\right) \tag{13}$$

with Boltzmann's constant k_B, a dimensionless cutoff-parameter ξ (see Appendix A), and normalization constant

$$N_{\mathrm{RKD}} = \frac{n}{\pi^{3/2}\,\kappa^{3/2}\,\mathcal{U}_0}\left(\frac{m}{2\,k_B\,T}\right)^{3/2}, \tag{14}$$

where $\mathcal{U}_0 \equiv \mathcal{U}(3/2,\, 3/2 - \kappa,\, \xi^2\kappa)$, $\mathcal{U}(a, b, x)$ being Kummer's function (see Appendices A and B). Furthermore, κ is a free parameter characterizing the suprathermal tails of the distribution function. Using this alternative form of f_{RKD}, we can rewrite Equation (12) in terms of f_1 to find

$$\begin{aligned} f_1 = &-\frac{f_{\mathrm{RKD}}\,(\kappa+1)}{\nu_{ei}(k_B\,T\,\kappa + \varepsilon)}\left(e\,\boldsymbol{E} + \frac{\varepsilon}{T}\nabla T\right)\cdot \boldsymbol{v} \\ &- \frac{f_{\mathrm{RKD}}\,\xi^2}{\nu_{ei}\,k_B\,T}\left(e\,\boldsymbol{E} + \frac{\varepsilon}{T}\nabla T\right)\cdot \boldsymbol{v} \\ &+ \frac{3}{2}\frac{f_{\mathrm{RKD}}}{\nu_{ei}}\frac{\nabla T}{T}\cdot \boldsymbol{v} - \frac{f_{\mathrm{RKD}}}{\nu_{ei}\,n}\nabla n \cdot \boldsymbol{v}. \end{aligned} \tag{15}$$

2.1. Diffusion Coefficient

The diffusion coefficient D is derived by setting $\boldsymbol{E} = \boldsymbol{0}$ and $\nabla T = \boldsymbol{0}$. Equation (15) then reduces to

$$f_1 = -\frac{f_{\mathrm{RKD}}}{\nu_{ei}\,n}\nabla n \cdot \boldsymbol{v}. \tag{16}$$

The particle flux in Equation (2) simplifies to

$$\boldsymbol{\Gamma} = \int d^3v\, \boldsymbol{v}\, f = \int d^3v\, \boldsymbol{v}\, f_1, \tag{17}$$

as $\int d^3v\, \boldsymbol{v}\, f_{\mathrm{RKD}} = 0$ due to the odd integrand with respect to the velocity. Inserting Equation (16) into (17) yields

$$\boldsymbol{\Gamma} = -\frac{1}{n}\int d^3v\, \frac{\boldsymbol{vv}}{\nu_{ei}} f_{\mathrm{RKD}}\nabla n = -\frac{1}{3\,n}\left\langle \frac{v^2}{\nu_{ei}}\right\rangle \nabla n. \tag{18}$$

The vanishing cross-diagonal terms in the dyadic product $\boldsymbol{vv}$ in Equation (18) allow one to rewrite the integral into $\int d^3v\, \boldsymbol{vv}\, G(v) = 1/3\, \mathcal{I} \int d^3v\, v^2\, G(v)$, where $\mathcal{I}$ denotes the unit tensor and $G(v)$ is some function of speed v. Then the integral can be transformed into an average value $\langle F(v)\rangle \equiv \int d^3v\, F(v) f_{\mathrm{RKD}}$, where $F(v)$ is some function of v. This procedure is performed for all considered transport coefficients in the present work.

By comparing Equations (18) and (1), we can identify the diffusion coefficient as

$$D = \frac{1}{3\,n}\left\langle \frac{v^2}{\nu_{ei}}\right\rangle = \frac{m^2}{12\,\pi\, z\, e^4\, L^{ei}\, n^2}\,\langle v^5\rangle. \tag{19}$$

Scherer et al. (2020) derived general solutions of integrals that contain (regularized) kappa distributions (see also Appendix B), and after solving the integral, we obtain the diffusion coefficient based on the RKD as

$$D = \underbrace{\frac{4\,\sqrt{2}\,(k_B\,T)^{5/2}}{m^{1/2}\,\pi^{3/2}\,n\,z\,e^4\,L^{ei}}}_{\equiv D_M}\frac{\kappa^{5/2}\,\mathcal{U}_{[4,4]}}{\mathcal{U}_0} = D_M\frac{\kappa^{5/2}\,\mathcal{U}_{[4,4]}}{\mathcal{U}_0}, \tag{20}$$

where D_M is the Maxwellian diffusion coefficient and where we made use of the compact notation given in Equation (B3), which is $\mathcal{U}_{[l,m]} \equiv \mathcal{U}(l,\, m - \kappa,\, \xi^2\kappa)$. By setting $\xi = 0$, Equation (20) becomes the diffusion coefficient based on the SKD (see Husidic et al. 2021 for all transport coefficients based on the SKD) as

$$D = D_M\frac{\Gamma(\kappa - 3)}{\Gamma(\kappa - 1/2)}\,\kappa^{5/2}. \tag{21}$$

From Equation (20) (as well as from all the subsequent transport coefficients below), we can see that the diffusion coefficient can be written as a product of a Maxwellian part and a κ-dependent part. This is a consequence of the composition of the RKD (see Scherer et al. 2020 for a detailed discussion), and enables a simple assessment of the influence of suprathermal particles on the transport coefficients.

Figure 1 shows the diffusion coefficient D as a function of κ and based on the SKD and three RKDs with different cutoff parameters (see legend). While the SKD-based result diverges approaching $\kappa = 3$, the RKD-based results resolve the singularity, allowing for a continuation to $\kappa < 3$. Furthermore, for increasing values of ξ, the values for D become smaller. The maximum value of the diffusion coefficient as well as for all other transport coefficients are presented in Appendix C.

2.2. Mobility Coefficient

The mobility coefficient μ in Equation (1) is obtained by setting $\nabla n = \boldsymbol{0}$ and $\nabla T = \boldsymbol{0}$. Equation (15) then becomes

$$f_1 = \left[-\frac{f_{\mathrm{RKD}}\,(\kappa+1)e}{\nu_{ei}(k_B\,T\,\kappa + \varepsilon)} - \frac{f_{\mathrm{RKD}}\,\xi^2\,e}{\nu_{ei}\,k_B\,T}\right]\boldsymbol{E}\cdot\boldsymbol{v}. \tag{22}$$

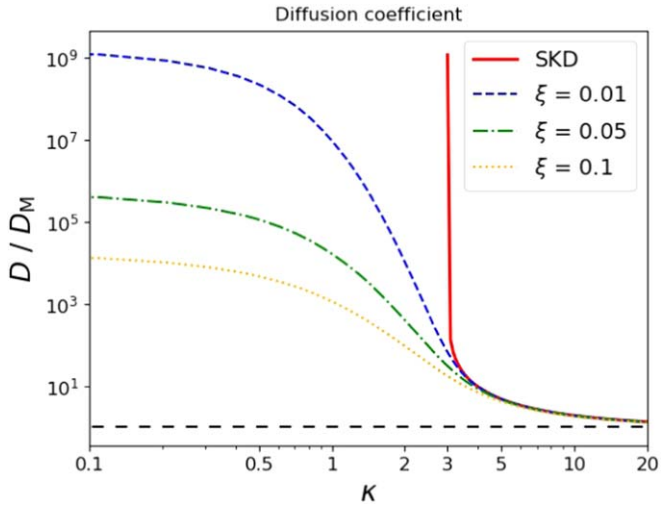

Figure 1. The plot displays the diffusion coefficient D as a function of κ. The curves show the results based on the SKD and three RKDs with different cutoff parameters (see legend). All functions are normalized to the Maxwellian limit (dashed horizontal line).

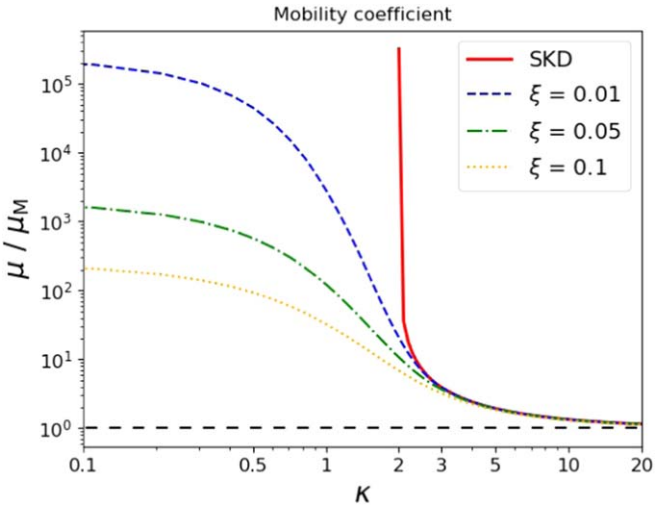

Figure 2. The plot displays the mobility coefficient μ as a function of κ. The curves show the results based on the SKD and three RKDs with different cutoff parameters (see legend). All functions are normalized to the Maxwellian limit (dashed horizontal line).

We can continue from Equation (17) and insert Equation (22) to obtain

$$\begin{aligned}\boldsymbol{\Gamma} &= -(\kappa+1)e\int d^3v\,\frac{\boldsymbol{vv}}{\nu_{\rm ei}}(k_{\rm B}\,T\,\kappa+\varepsilon)^{-1}f_{\rm RKD}\,\boldsymbol{E}\\ &\quad-\frac{\xi^2\,e}{k_{\rm B}\,T}\int d^3v\,\frac{\boldsymbol{vv}}{\nu_{\rm ei}}f_{\rm RKD}\,\boldsymbol{E}\\ &=\left[-\frac{(\kappa+1)e}{3}\left\langle\frac{v^2}{\nu_{\rm ei}}(k_{\rm B}\,T\,\kappa+\varepsilon)^{-1}\right\rangle\right.\\ &\quad\left.-\frac{\xi^2\,e}{3\,k_{\rm B}\,T}\left\langle\frac{v^2}{\nu_{\rm ei}}\right\rangle\right]\boldsymbol{E}.\end{aligned}\tag{23}$$

Comparing Equations (23) and (1) allows one to identify the mobility coefficient as

$$\mu=\frac{(\kappa+1)e}{3\,n}\left\langle\frac{v^2}{\nu_{\rm ei}}(k_{\rm B}\,T\,\kappa+\varepsilon)^{-1}\right\rangle+\frac{\xi^2\,e}{3\,k_{\rm B}\,T\,n}\left\langle\frac{v^2}{\nu_{\rm ei}}\right\rangle.\tag{24}$$

We insert the expression for the collision frequency from Equation (11) and introduce the quantity $A_\kappa\equiv m/(k_{\rm B}\,T\,\kappa)$, which leads to

$$\begin{aligned}\mu&=\frac{(\kappa+1)m^2}{12\,\pi\,n^2\,k_{\rm B}\,T\,\kappa\,z\,e^3\,L_{\rm ei}}\left\langle v^5(1+A_\kappa\,v^2)^{-1}\right\rangle\\ &\quad+\frac{\xi^2\,m^2}{12\,\pi\,n^2\,k_{\rm B}\,T\,z\,e^3\,L_{\rm ei}}\left\langle v^5\right\rangle.\end{aligned}\tag{25}$$

After solving the integrals (see Appendix B), the mobility coefficient based on the RKD takes the form

$$\begin{aligned}\mu&=\underbrace{\frac{4\,\sqrt{2}\,(k_{\rm B}\,T)^{3/2}}{m^{1/2}\,\pi^{3/2}\,n\,z\,e^3\,L}}_{\equiv\,\mu_{\rm M}}\frac{\kappa^{3/2}}{\mathcal{U}_0}[(\kappa+1)\mathcal{U}_{[4,3]}+\kappa\,\xi^2\,\mathcal{U}_{[4,4]}]\\ &=\mu_{\rm M}\,\frac{\kappa^{3/2}}{\mathcal{U}_0}[(\kappa+1)\mathcal{U}_{[4,3]}+\kappa\,\xi^2\,\mathcal{U}_{[4,4]}],\end{aligned}\tag{26}$$

where $\mu_{\rm M}$ is the Maxwellian mobility coefficient. With $\xi=0$, Equation (26) becomes the mobility coefficient based on the SKD

$$\mu=\mu_{\rm M}\frac{\Gamma(\kappa-2)}{\Gamma(\kappa-1/2)}\,\kappa^{3/2}.\tag{27}$$

The Einstein equation, which establishes the relationship between the diffusion and mobility coefficients, is obtained by combining Equations (20) and (26), yielding

$$D=\frac{\kappa\,\mathcal{U}_{[4,4]}}{(\kappa+1)\mathcal{U}_{[4,3]}+\kappa\,\xi^2\,\mathcal{U}_{[4,4]}}\,\frac{\mu\,k_{\rm B}\,T}{e}.\tag{28}$$

By setting $\xi=0$, this equation can be simplified to the case for the SKD

$$D=\frac{\kappa}{\kappa-3}\,\frac{\mu\,k_{\rm B}\,T}{e},\tag{29}$$

and with $\kappa\to\infty$ further simplified to the well-known Maxwellian-based result $D_{\rm M}=\mu_{\rm M}\,k_{\rm B}\,T/e$. The estimates of the mobility coefficient for three RKDs with different cutoff parameters, and the corresponding SKD, are displayed in Figure 2. The result based on the SKD diverges at $\kappa=2$, whereas the RKD-based results continue to lower values of κ. By increasing the cutoff-parameter ξ, the value of the mobility coefficient becomes smaller.

2.3. The Electric Conductivity

Similarly to the mobility coefficient, we set $\nabla n=\mathbf{0}$ and $\nabla T=\mathbf{0}$ to calculate the electric conductivity. We find for f_1 the same expression as in Equation (22), which we then insert in Equation (4) to find

$$\boldsymbol{j}=-e\int d^3v\,\boldsymbol{v}\,f=-e\int d^3v\,\boldsymbol{v}\,f_1.\tag{30}$$

Equation (30) differs from Equation (17) only in an additional factor $-e$, leading to the same integrals as in Equation (23). Thus, using Equation (3), we can immediately write the electric conductivity based on the RKD as

$$\sigma = \underbrace{\frac{4\sqrt{2}\,(k_B\,T)^{3/2}}{m^{1/2}\,\pi^{3/2}\,z\,e^2\,L}}_{\equiv\,\sigma_M}\frac{\kappa^{3/2}}{\mathcal{U}_0}[(\kappa+1)\mathcal{U}_{[4,3]}+\kappa\,\xi^2\,\mathcal{U}_{[4,4]}]$$
$$= \sigma_M\frac{\kappa^{3/2}}{\mathcal{U}_0}[(\kappa+1)\mathcal{U}_{[4,3]}+\kappa\,\xi^2\,\mathcal{U}_{[4,4]}] \tag{31}$$

with σ_M being the Maxwellian electric conductivity. The relation between σ and μ is

$$\sigma = n\,e\,\mu. \tag{32}$$

We set $\xi = 0$ to obtain the SKD-based result for σ with

$$\sigma = \sigma_M\frac{\Gamma(\kappa-2)}{\Gamma(\kappa-1/2)}\,\kappa^{3/2}. \tag{33}$$

Figure 3 shows the electric conductivity as a function of κ for three different RKDs and, to compare, the corresponding SKD. Since $\sigma/\sigma_M = \mu/\mu_M$ (see Equation (26)), the relative values obtained in this case are exactly the same as those displayed for the mobility coefficient in Figure 2.

2.4. The Thermoelectric Coefficient

The thermoelectric coefficient is derived by setting $\boldsymbol{E} = \boldsymbol{0}$ and $\nabla n = \boldsymbol{0}$, which simplifies Equation (15) to

$$f_1 = \left[-\frac{f_{RKD}\,(\kappa+1)\varepsilon}{\nu_{ei}(k_B\,T\,\kappa+\varepsilon)} - \frac{f_{RKD}\,\xi^2\,\varepsilon}{k_B\,T\,\nu_{ei}} + \frac{3}{2}\frac{f_\kappa}{\nu_{ei}}\right]\frac{\nabla T}{T}\cdot\boldsymbol{v}. \tag{34}$$

We insert Equation (34) into (30) to obtain

$$\boldsymbol{j} = \frac{(\kappa+1)e}{T}\nabla T\cdot\int d^3v\,\frac{\boldsymbol{vv}}{\nu_{ei}}(k_B\,T\,\kappa+\varepsilon)^{-1}\varepsilon\,f_\kappa$$
$$+\frac{\xi^2\,e}{k_B\,T^2}\nabla T\cdot\int d^3v\,\frac{\boldsymbol{vv}}{\nu_{ei}}\,\varepsilon\,f_\kappa$$
$$-\frac{3}{2}\frac{e}{T}\nabla T\cdot\int d^3v\,\frac{\boldsymbol{vv}}{\nu_{ei}}f_\kappa$$
$$=\left[\frac{(\kappa+1)e}{3\,T}\left\langle\frac{v^2\,\varepsilon}{\nu_{ei}}(k_B\,T\,\kappa+\varepsilon)^{-1}\right\rangle\right.$$
$$\left.+\frac{\xi^2\,e}{3\,k_B\,T^2}\left\langle\frac{v^2\,\varepsilon}{\nu_{ei}}\right\rangle-\frac{e}{2\,T}\left\langle\frac{v^2}{\nu_{ei}}\right\rangle\right]\nabla T. \tag{35}$$

By comparing the coefficients in Equations (35) and (3), we are able to identify the thermoelectric coefficient as

$$\alpha = -\frac{(\kappa+1)e}{3\,T\,\sigma}\left\langle\frac{v^2\,\varepsilon}{\nu_{ei}}(k_B\,T\,\kappa+\varepsilon)^{-1}\right\rangle$$
$$-\frac{\xi^2\,e}{3\,k_B\,T^2\,\sigma}\left\langle\frac{v^2\,\varepsilon}{\nu_{ei}}\right\rangle+\frac{e}{2\,T\,\sigma}\left\langle\frac{v^2}{\nu_{ei}}\right\rangle. \tag{36}$$

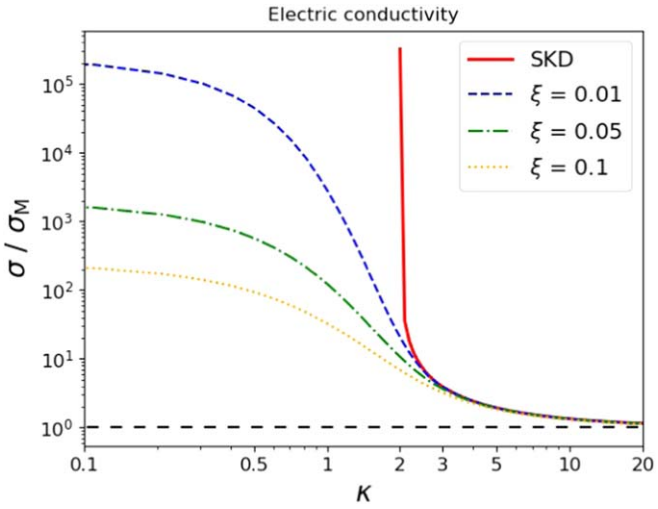

Figure 3. The plot displays the electric conductivity σ as a function of κ. The curves show the results based on the SKD and three RKDs with different cutoff parameters (see legend). All functions are normalized to the Maxwellian limit (dashed horizontal line).

We insert the expression for the collision frequency from Equation (11) into the equation above to obtain

$$\alpha = -\frac{(\kappa+1)m^3}{24\,\pi\,n\,z\,e^3\,k_B\,T^2\,\kappa\,L_{ei}\,\sigma}\langle v^7(1+A_\kappa\,v^2)^{-1}\rangle$$
$$-\frac{\xi^2\,m^3}{24\,\pi\,n\,z\,e^3\,k_B\,T^2\,L_{ei}\,\sigma}\langle v^7\rangle$$
$$+\frac{m^2}{8\,\pi\,n\,z\,e^3\,T\,L_{ei}\,\sigma}\langle v^5\rangle. \tag{37}$$

Solving the integrals and inserting the found expression for σ from Equation (31) yields the thermoelectric coefficient based on the RKD in the form

$$\alpha = -\underbrace{\frac{5\,k_B}{2\,e}}_{\equiv\,\alpha_M}\frac{\kappa\left[4(\kappa+1)\mathcal{U}_{[5,4]}-\frac{3}{2}\mathcal{U}_{[4,4]}+4\,\kappa\,\xi^2\,\mathcal{U}_{[5,5]}\right]}{5/2[(\kappa+1)\mathcal{U}_{[4,3]}+\kappa\,\xi^2\,\mathcal{U}_{[4,4]}]}$$
$$=\alpha_M\frac{\kappa\left[4(\kappa+1)\mathcal{U}_{[5,4]}-\frac{3}{2}\mathcal{U}_{[4,4]}+4\,\kappa\,\xi^2\,\mathcal{U}_{[5,5]}\right]}{5/2[(\kappa+1)\mathcal{U}_{[4,3]}+\kappa\,\xi^2\,\mathcal{U}_{[4,4]}]} \tag{38}$$

with the Maxwellian thermoelectric coefficient α_M. Furthermore, with $\xi = 0$, the SKD-based result for α becomes

$$\alpha = \alpha_M\frac{\kappa}{\kappa-3}. \tag{39}$$

Figure 4 displays the thermoelectric coefficient as a function of κ. Similarly to the previous transport coefficients, we see that the SKD-based result has a singularity (here at $\kappa = 3$), which is resolved by the RKD.

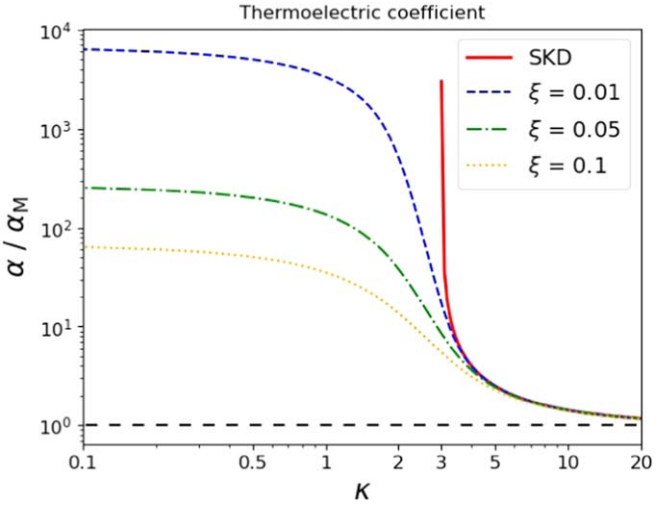

Figure 4. The plot displays the thermoelectric coefficient α as a function of κ. The results are based on the SKD and three RKDs with different cutoff parameters (see legend). All functions are normalized to the Maxwellian limit (dashed horizontal line).

2.5. The Thermal Conductivity

For the the derivation of the thermal conductivity, we set $\nabla n = \mathbf{0}$ and assume the absence of an electric current ($\boldsymbol{j} = \mathbf{0}$), which simplifies Equation (3) to $\boldsymbol{E} = \alpha \nabla T$. Equation (15) then becomes

$$f_1 = -\frac{f_\kappa(\kappa+1)(\alpha\, e + \varepsilon/T)}{\nu_{ei}(k_B\, T\, \kappa + \varepsilon)} \nabla T \cdot \boldsymbol{v} - \frac{f_\kappa\, \xi^2 (\alpha\, e + \varepsilon/T)}{\nu_{ei}\, k_B\, T} \nabla T \cdot \boldsymbol{v} + \frac{3}{2}\frac{f_\kappa}{\nu_{ei}}\frac{\nabla T}{T} \cdot \boldsymbol{v}, \quad (40)$$

which we insert into Equation (6) to obtain

$$\begin{aligned}\boldsymbol{q} &= -(\kappa+1)\int d^3v\, \frac{\boldsymbol{vv}}{\nu_{ei}} \frac{(\alpha\, e + \varepsilon/T)\varepsilon\, f_\kappa}{k_B\, T\, \kappa + \varepsilon} \nabla T \\ &\quad - \frac{\xi^2}{k_B\, T}\int d^3v\, \frac{\boldsymbol{vv}}{\nu_{ei}} (\alpha\, e + \varepsilon/T)\varepsilon\, f_\kappa\, \nabla T \\ &\quad + \frac{3}{2\, T}\int d^3v\, \frac{\boldsymbol{vv}}{\nu_{ei}} \varepsilon\, f_\kappa\, \nabla T \\ &= \left[-\frac{\kappa+1}{3}\left\langle \frac{v^2}{\nu_{ei}} \frac{(\alpha\, e + \varepsilon/T)\varepsilon}{k_B\, T\, \kappa + \varepsilon} \right\rangle \right. \\ &\quad \left. - \frac{\xi^2}{3\, k_B\, T}\left\langle \frac{v^2}{\nu_{ei}} (\alpha\, e + \frac{\varepsilon}{T})\varepsilon \right\rangle + \frac{1}{2\, T}\left\langle \frac{v^2}{\nu_{ei}}\varepsilon \right\rangle \right] \nabla T. \end{aligned} \quad (41)$$

A comparison of the coefficients in Equations (41) and (5) leads for the thermal conductivity to the expression

$$\lambda = \frac{\kappa+1}{3}\left\langle \frac{v^2}{\nu_{ei}} \frac{(\alpha\, e + \varepsilon/T)\varepsilon}{k_B\, T\, \kappa + \varepsilon} \right\rangle + \frac{\xi^2}{3\, k_B\, T}\left\langle \frac{v^2}{\nu_{ei}} \left(\alpha\, e + \frac{\varepsilon}{T}\right)\varepsilon \right\rangle - \frac{1}{2\, T}\left\langle \frac{v^2}{\nu_{ei}}\varepsilon \right\rangle. \quad (42)$$

We plug the collision frequency from Equation (11) into the equation above to find

$$\begin{aligned}\lambda &= \frac{(\kappa+1)\alpha\, m^3}{24\, \pi\, n\, z\, e^3\, L_{ei}\, k_B\, T\, \kappa} \langle v^7 (1 + A_\kappa\, v^2)^{-1} \rangle \\ &\quad + \frac{(\kappa+1) m^4}{48\, \pi\, n\, z\, e^4\, L_{ei}\, k_B\, T^2\, \kappa} \langle v^9 (1 + A_\kappa\, v^2)^{-1} \rangle \\ &\quad + \frac{\xi^2\, \alpha\, m^3}{24\, \pi\, n\, z\, e^3\, L_{ei}\, k_B\, T} \langle v^7 \rangle + \frac{\xi^2\, m^4}{48\, \pi\, n\, z\, e^4\, L_{ei}\, k_B\, T^2} \langle v^9 \rangle \\ &\quad - \frac{m^3}{16\, \pi\, n\, z\, e^4\, L_{ei}\, T} \langle v^7 \rangle. \end{aligned} \quad (43)$$

After solving the integrals and inserting the thermoelectric coefficient from Equation (38), we obtain the thermal conductivity λ based on the RKD, reading

$$\begin{aligned}\lambda &= \underbrace{\frac{16\sqrt{2}\, k_B (k_B\, T)^{5/2}}{m^{1/2}\, \pi^{3/2}\, z\, e^4\, L}}_{\equiv \lambda_M} \frac{\kappa^{7/2}}{\mathcal{U}_0} \\ &\quad \times \left[5(\kappa+1)\mathcal{U}_{[6,5]} + 5\, \xi^2\, \kappa\, \mathcal{U}_{[6,6]} \right. \\ &\quad - \frac{3}{2}\mathcal{U}_{[5,5]} - [(\kappa+1)\mathcal{U}_{[5,4]} + \xi^2\, \kappa\, \mathcal{U}_{[5,5]}] \\ &\quad \left. \times \frac{4(\kappa+1)\mathcal{U}_{[5,4]} - \frac{3}{2}\mathcal{U}_{[4,4]} + 4\, \kappa\, \xi^2\, \mathcal{U}_{[5,5]}}{(\kappa+1)\mathcal{U}_{[4,3]} + \kappa\, \xi^2\, \mathcal{U}_{[4,4]}} \right]. \end{aligned} \quad (44)$$

Setting $\xi = 0$ yields λ based on the SKD as

$$\lambda = \lambda_M \frac{\Gamma(\kappa-4)}{\Gamma(\kappa-1/2)} \frac{\kappa^{7/2}(\kappa-1/2)}{(\kappa-3)}. \quad (45)$$

Figure 5 shows the thermal conductivity as a function of κ and with the same composition as the previous figures. While the SKD-based result has a singularity at $\kappa = 4$, the RKD removes the pole and allows λ to continue to values $\kappa < 4$.

3. Conclusions and Outlook

The results presented in this paper respond to the current high interest to evaluate transport coefficients in non-equilibrium space plasmas, where the effects of Coulomb collisions are counter-balanced by the interactions of plasma particles with the wave turbulence and fluctuations. It seems that this interplay can also offer a plausible explanation for the observed kappa-like distribution of particle velocities (Yoon 2011; Bian et al. 2014), a distribution that is nearly Maxwellian at low energies, but decreases as a power law with increasing energies (up to a few keV; Pierrard & Lazar 2010). A macroscopic description of these plasmas depends on the nature of particle velocity distributions, and in this case, it should rely on kappa distribution models. However, macroscopic velocity moments of SKDs (Olbert 1968; Vasyliūnas 1968), such as pressure, temperature, and heat flux, cannot be defined for distributions with hard suprathermal tails, i.e., low power exponents $\kappa \leqslant 3/2$ (Lazar et al. 2020). Moreover, recent derivations of transport coefficients for SKD electrons have shown that their mobility and electric conductivity cannot be defined for $\kappa \leqslant 2$, the diffusion coefficient and thermoelectric coefficient become divergent for $\kappa \leqslant 3$, and the thermal conductivity for $\kappa \leqslant 4$ (Husidic et al. 2021).

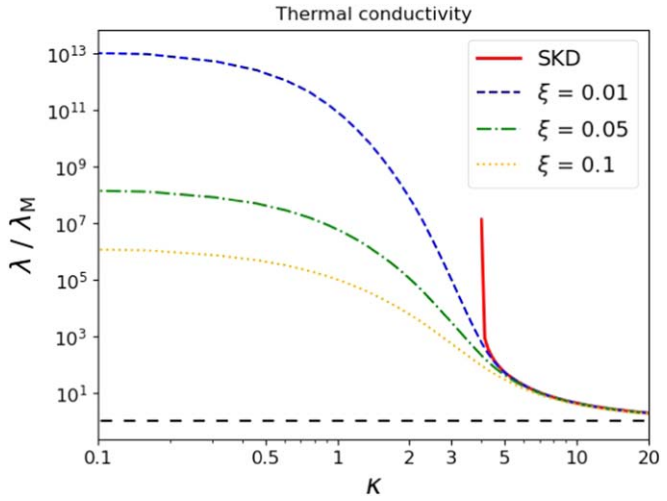

Figure 5. The plot displays the thermal conductivity λ as a function of κ. The curves show the results based on the SKD and three RKDs with different cutoff parameters (see legend). All functions are normalized to the Maxwellian limit (dashed horizontal line).

In this paper, we derived new expressions of these transport coefficients assuming the electrons described by an RKD that has the merit to resolve all these mathematical divergences and enable a well-defined macroscopic parameterization (Scherer et al. 2017). It also reduces the unphysical contributions of superluminal electrons from the tails of an SKD (Scherer et al. 2019). All macroscopic parameters, including the transport coefficients mentioned above, are found to be well defined for all values of $\kappa > 0$. Moreover, for low values of the power exponent κ, i.e., below the SKD poles, values obtained for the transport coefficients can be markedly higher, order of magnitudes higher than the corresponding Maxwellian limits. That means that transport coefficients can be significantly underestimated if evaluated in the absence of suprathermal electrons. For instance, even for a moderate presence of suprathermals, i.e., for $\kappa = 2.5$, and a fair cutoff, i.e., $\xi = 0.05$, we obtain $\mu/\mu_{\rm M} \approx 5.5$ for mobility (and the same for electric conductivity σ), $\alpha/\alpha_{\rm M} \approx 17.6$ for thermoelectric coefficient, and much higher differences, like $D/D_{\rm M} \approx 93.4$ for the diffusion coefficient or $\lambda/\lambda_{\rm M} \approx 1.7 \times 10^4$ for the thermal conductivity.

The choice of ξ in the above numerical example is somewhat arbitrary and follows mainly the requirements that $\xi > \Theta/c$ and that the essential property of kappa distributions is retained, namely the consideration of a sufficient number of suprathermal particles. The sensitivity of the solutions for the transport coefficients to the value of ξ becomes obvious if ξ is slightly varied. For instance, if we consider the diffusion coefficient from the numerical example from above with $\kappa = 2.5$ and increase ξ to 0.06, $D/D_{\rm M}$ is reduced by a factor of about 1.26. For smaller values of κ, this factor increases, e.g., for the limit $\kappa \to 0$, by a factor of about 2.49. However, this sensitivity is not an artifact of the RKD. It rather expresses the physical fact that the diffusion coefficient, when calculated with the standard definition used, depends critically on the cutoff of a distribution function, which it must have. We note that the advantage of the RKD holds nonetheless. Using an SKD, κ values below 3—which frequently occur in the solar wind—would not be accessible at all, as the diffusion coefficient diverges. However, using an RKD, it is reduced to finite values. Furthermore, the sensitivity of the diffusion coefficient with respect to κ is extreme for the SKD when approaching the critical value of 3, while for the RKD it is more reduced and getting successively smaller with the decreasing κ. These advantages outweigh the high sensitivity with respect to ξ even if one would not accept it as a consequence of a distribution's cutoff. In addition, it is unclear whether observations can reveal such subtle differences in the ξ-parameter.

We conclude by reaffirming that, based on the RKD models, realistic and physically well-defined parameterizations of the observed non-equilibrium plasmas become possible now. Future studies should confront our results with the estimations of these transport coefficients from a direct numerical integration of observational data. The best RKD fit must be conditioned only by the observed velocity distribution, without any theoretical restriction for the power exponent κ.

The authors acknowledge support from the Ruhr-University Bochum and the Katholieke Universiteit Leuven. E.H. is grateful to the Space Weather Awareness Training Network (SWATNet) funded by the European Union's Horizon 2020 research and innovation program under the Marie Skłodowska-Curie grant agreement No. 955620. M.L. and H.F. are grateful for support by the German Research Foundation (Deutsche Forschungsgemeinschaft, DFG) through project SCHL 201/35-1. Furthermore, these results were obtained in the framework of the projects C14/19/089 (C1 project Internal Funds KU Leuven), G.0D07.19N (FWO-Vlaanderen), SIDC Data Exploitation (ESA Prodex-12), and Belspo projects BR/165/A2/CCSOM and B2/191/P1/SWiM. The authors thank the anonymous referee for helpful remarks.

Appendix A
RKD versus SKD

The RKD can be seen as a generalization of the SKD and was introduced by Scherer et al. (2017) in the form

$$f_{\rm RKD} = \frac{n}{\pi^{3/2}\,\Theta^3\,\kappa^{3/2}\,\mathcal{U}_0}\left(1+\frac{v^2}{\kappa\,\Theta^2}\right)^{-(\kappa+1)} \times \exp\left(-\xi^2\frac{v^2}{\Theta^2}\right), \tag{A1}$$

where $\mathcal{U}(a, b, x)$ is Kummer's function (see, e.g., Abramowitz & Stegun 1970) and $\mathcal{U}_0 \equiv \mathcal{U}(3/2, 3/2-\kappa, \xi^2\kappa)$. Furthermore, n is the particle number density, v is the individual particle speed, and κ is a free parameter characterizing the high-energy tails of the distribution. The variable Θ is often termed the thermal speed and can be, in principal, included either as a constant speed determined by observations, or as an analytical expression. In order to compare the results obtained for an RKD, an SKD, and a Maxwellian, we choose the latter variant and use for Θ the Maxwellian thermal speed $\Theta = \sqrt{2\,k_{\rm B}\,T/m}$ with Boltzmann's constant $k_{\rm B}$, corresponding Maxwellian temperature T, and particle mass m. The cutoff-parameter ξ has to fulfill the relation $\xi > \Theta/c$ (Scherer et al. 2019) with vacuum speed of light c, but must be small enough to retain the main implication of the distribution. By setting $\xi = 0$, the SKD is recovered, and Equation (A1) becomes

$$f_{\rm SKD} = \frac{n}{\pi^{3/2}\,\Theta^3}\frac{\Gamma(\kappa+1)}{\kappa^{3/2}\,\Gamma(\kappa-1/2)}\left(1+\frac{v^2}{\kappa\,\Theta^2}\right)^{-(\kappa+1)}, \tag{A2}$$

where $\Gamma(x)$ is the (complete) gamma function of some argument x. If additionally $\kappa \to \infty$, the Maxwellian distribution

$$f_{\rm MD} = \frac{n}{\pi^{3/2}\,\Theta^3}\exp\left(-\frac{v^2}{\Theta^2}\right) \tag{A3}$$

is acquired.

Appendix B
Useful Formulas and Integrals

In this appendix, we present useful definitions, relations, and general formulas for the calculations in Section 2, which can be found in Abramowitz & Stegun (1970), Oldham et al. (2009), and Scherer et al. (2020). Kummer's function belongs to the confluent hypergeometric functions and can be represented in integral form as

$$\mathcal{U}(a,\,b,\,x) = \frac{1}{\Gamma(a)}\int_0^\infty dt\,\exp(-x\,t)\,t^{\,a-1}(1\,+\,t)^{b-a-1} \quad \text{with } a > 0,\, x > 0. \tag{B1}$$

The case $a = 0$ leads to $\mathcal{U}(0,\,b,\,x) = 1, \forall\, b,\, x \in \mathbb{R}$, while $x = 0$ not always yields finite solutions. However, if $b \leqslant 1$ and $x = 0$, then

$$\mathcal{U}(a,\,b,\,0) = \frac{\Gamma(1\,-\,b)}{\Gamma(1\,+\,a\,-\,b)}, \tag{B2}$$

which can be used to transform the RKD (Equation (A1)) into the SKD (Equation (A2)). For a compact notation of the transport coefficients in Section 2, we further introduce the definition

$$\mathcal{U}_{[l,m]} \equiv \mathcal{U}(l,\,m\,-\,\kappa,\,\xi^2\kappa). \tag{B3}$$

The integrals in Section 2, which calculate the $n-$th moment M_n of the RKD, are of type

$$M_n = \langle v^n\,(1\,+\,A_\kappa\,v^2)^\eta\rangle = 4\,\pi\,N_\kappa\int_0^\infty dv\,v^{\,n+2}(1\,+\,A_\kappa v^2)^{-\zeta}\exp\left(-\xi^2\frac{v^2}{\Theta^2}\right) \tag{B4}$$

with $4\,\pi$ being the solution of the integrals over θ and ϕ, η being either -1 or 0, and ζ being either $\kappa+1$ or $\kappa+2$ in the integrals in Section 2. General solutions are given by Scherer et al. (2020) and read

$$M_n = 2\,\pi\,\kappa^{\frac{3+n}{2}}\,\Theta^{3+n} \times \Gamma\left(\frac{3\,+\,n}{2}\right)\mathcal{U}\left(\frac{3\,+\,n}{2},\,\frac{3\,+\,n}{2}\,-\,\zeta,\,\xi^2\,\kappa\right). \tag{B5}$$

And thus $m = l$ or $m = l+1$ in Equation (B3). Using Equations (B4) and (B5), we obtain the following solutions for the integrals in Section 2:

$$\langle v^5\,(1\,+\,A_\kappa\,v^2)^{-1}\rangle = 12\,\pi\,\Theta^8\,\kappa^4\,\mathcal{U}(4,\,3\,-\,\kappa,\,\xi^2\kappa) \tag{B6}$$

$$\langle v^7\,(1\,+\,A_\kappa\,v^2)^{-1}\rangle = 48\,\pi\,\Theta^{10}\,\kappa^5\,\mathcal{U}(5,\,4\,-\,\kappa,\,\xi^2\kappa) \tag{B7}$$

$$\langle v^9\,(1\,+\,A_\kappa\,v^2)^{-1}\rangle = 240\,\pi\,\Theta^{12}\,\kappa^6\,\mathcal{U}(6,\,5\,-\,\kappa,\,\xi^2\kappa) \tag{B8}$$

$$\langle v^5\rangle = 12\,\pi\,\Theta^8\,\kappa^4\,\mathcal{U}(4,\,4\,-\,\kappa,\,\xi^2\kappa) \tag{B9}$$

$$\langle v^7\rangle = 48\,\pi\,\Theta^{10}\,\kappa^5\,\mathcal{U}(5,\,5\,-\,\kappa,\,\xi^2\kappa) \tag{B10}$$

$$\langle v^9\rangle = 240\,\pi\,\Theta^{12}\,\kappa^6\,\mathcal{U}(6,\,6\,-\,\kappa,\,\xi^2\kappa) \tag{B11}$$

For the derivation of the maximum values of the transport coefficients in the limit $\kappa \to 0$, the following relations are helpful and are taken from Table A1 of Scherer et al. (2020):

$$\mathcal{U}(a,\,b,\,\xi^2\,\kappa) = \frac{\Gamma(c\,-\,1)}{\Gamma(a)(\xi^2\,\kappa)^{\,c-1}} + \frac{\Gamma(1\,-\,c)}{\Gamma(\kappa\,+\,1)} \qquad \text{for } 1 < b < 2, \tag{B12}$$

$$\mathcal{U}(a,\,b,\,\xi^2\,\kappa) = \frac{(d\,-\,2\,-\,(\kappa\,+\,1)\xi^2\,\kappa)\Gamma(c\,-\,2)}{\Gamma(a)(\xi^2\,\kappa)^{c-1}} \qquad \text{for } b > 2, \tag{B13}$$

where $a = (3+n)/2$, $b = (3+n-2\,\kappa)/2$, $d = 1+a-b$, and moment $n \in \mathbb{N}_0$.

Appendix C
Tabulated Transport Coefficients and Their Limits for $\kappa \to 0$

The RKD is well defined for all $\kappa > 0$. While $\kappa = 0$ cannot be directly inserted into Kummer's function, the continuation $\kappa \to 0$ is still possible by using approximations. Thus, for the purpose of mathematical completeness, we derive the maximum values of the transport coefficients under consideration, which are obtained in the limit $\kappa \to 0$ (and $\xi > 0$). We begin by recognizing that small but finite κ-values and finite ξ-values enable to make the following approximations for $\mathcal{U}_0$ and $\mathcal{U}_{[l,m]}$:

$$\mathcal{U}\left(\frac{3}{2},\,\frac{3}{2}\,-\,\kappa,\,\xi^2\kappa\right) \underset{\kappa\ll 1}{\approx} \mathcal{U}\left(\frac{3}{2},\,\frac{3}{2},\,\xi^2\kappa\right), \tag{C1}$$

$$\mathcal{U}(l,\,m\,-\,\kappa,\,\xi^2\kappa) \underset{\kappa\ll 1}{\approx} \mathcal{U}(l,\,m,\,\xi^2\kappa), \qquad \text{for } m > 2. \tag{C2}$$

We then may apply Equation (B12) to Equation (C1) and Equation (B13) to Equation (C2) in order to obtain

$$\mathcal{U}\left(\frac{3}{2},\,\frac{3}{2},\,\xi^2\kappa\right) = \frac{\Gamma\left(\frac{1}{2}\right)}{\Gamma\left(\frac{3}{2}\right)(\xi^2\kappa)^{1/2}} + \frac{\Gamma\left(-\frac{1}{2}\right)}{\Gamma(\kappa\,+\,1)}, \tag{C3}$$

$$\mathcal{U}(l,\,m,\,\xi^2\kappa) = \frac{[m\,-\,2\,-\,(\kappa\,+\,1)\xi^2\kappa]\,\Gamma(m\,-\,2)}{\Gamma(l)(\xi^2\kappa)^{\,m-1}}. \tag{C4}$$

We begin with the diffusion coefficient, where the approximation yields

$$\frac{D}{D_{\rm M}} = \frac{\kappa^{5/2}\,\mathcal{U}_{[4,4]}}{\mathcal{U}_0} \underset{\kappa\ll 1}{\approx} \frac{2\,-\,\xi^2\kappa}{6\,\xi^5}\frac{\Gamma\left(\frac{3}{2}\right)}{\Gamma\left(\frac{1}{2}\right) + \Gamma\left(-\frac{1}{2}\right)\Gamma\left(\frac{3}{2}\right)(\xi^2\kappa)^{1/2}}. \tag{C5}$$

In the limit $\kappa \to 0$, we then obtain

$$\lim_{\kappa\,\to\,0}\frac{D}{D_{\rm M}} = \frac{1}{6\,\xi^5}. \tag{C6}$$

This result is in agreement with Figure 1 for $\xi \in \{0.01,\, 0.05,\, 0.1\}$.

For both the mobility coefficient and the electric conductivity, we obtain the same expression, which reads

$$\frac{\mu}{\mu_{\rm M}} = \frac{\sigma}{\sigma_{\rm M}} = \frac{\kappa^{3/2}}{\mathcal{U}_0}[(\kappa+1)\mathcal{U}_{[4,3]} + \kappa\,\xi^2\,\mathcal{U}_{[4,4]}] \approx_{\kappa\ll 1} \frac{3-2\,\xi^2\kappa}{6\,\xi^3}\frac{\Gamma\left(\frac{3}{2}\right)}{\Gamma\left(\frac{1}{2}\right)+\Gamma\left(-\frac{1}{2}\right)\Gamma\left(\frac{3}{2}\right)(\xi^2\kappa)^{1/2}}, \tag{C7}$$

which becomes in the limit $\kappa \to 0$

$$\lim_{\kappa\to 0}\frac{\mu}{\mu_{\rm M}} = \lim_{\kappa\to 0}\frac{\sigma}{\sigma_{\rm M}} = \frac{1}{4\,\xi^3}. \tag{C8}$$

We refer to Figures 2 and 3 for a comparison of the maximum values for $\xi \in \{0.01, 0.05, 0.1\}$.

The thermoelectric coefficient can be written for $\kappa \ll 1$ as

$$\frac{\alpha}{\alpha_{\rm M}} = \frac{\kappa}{5}\frac{8(\kappa+1)\mathcal{U}_{[5,4]} - 3\,\mathcal{U}_{[4,4]} + 8\,\xi^2\kappa\,\mathcal{U}_{[5,5]}}{(\kappa+1)\mathcal{U}_{[4,3]} + \xi^2\,\kappa\,\mathcal{U}_{[4,4]}} \approx_{\kappa\ll 1} \frac{6}{3-2\,\xi^2\kappa}\times\left(\frac{2-\xi^2\kappa}{15\,\xi^2} - \frac{2-\xi^2\kappa}{10\,\xi^2} + \frac{6-2\,\xi^2\kappa}{15\,\xi^2}\right), \tag{C9}$$

which yields for limit $\kappa \to 0$

$$\lim_{\kappa\to 0}\frac{\alpha}{\alpha_{\rm M}} = \frac{2}{3\,\xi^2}. \tag{C10}$$

This result is in agreement with the corresponding plot in Figure 4 for $\xi \in \{0.01, 0.05, 0.1\}$.

Finally, the thermal conductivity can be approximated as

$$\begin{aligned}\frac{\lambda}{\lambda_{\rm M}} = \frac{\kappa^{7/2}}{\mathcal{U}_0}\Bigg[&5(\kappa+1)\mathcal{U}_{[6,5]} + 5\,\xi^2\,\kappa\,\mathcal{U}_{[6,6]} - \frac{3}{2}\,\mathcal{U}_{[5,5]} - [(\kappa+1)\mathcal{U}_{[5,4]} + \xi^2\,\kappa\,\mathcal{U}_{[5,5]}] \\ &\times\frac{4(\kappa+1)\mathcal{U}_{[5,4]} - \frac{3}{2}\,\mathcal{U}_{[4,4]} + 4\,\kappa\,\xi^2\,\mathcal{U}_{[5,5]}}{(\kappa+1)\mathcal{U}_{[4,3]} + \kappa\,\xi^2\,\mathcal{U}_{[4,4]}}\Bigg] \\ \approx_{\kappa\ll 1}&\frac{\Gamma\left(\frac{3}{2}\right)}{\Gamma\left(\frac{1}{2}\right)+\Gamma\left(-\frac{1}{2}\right)\Gamma\left(\frac{3}{2}\right)(\xi^2\kappa)^{1/2}} \\ &\times\Bigg\{\frac{3-\xi^2\kappa}{12\,\xi^7} + \frac{4-\xi^2\kappa}{4\,\xi^7} - \frac{3-\xi^2\kappa}{8\,\xi^7} - \frac{8-3\,\xi^2\kappa}{24\,\xi^7} \\ &\times\frac{6}{3-2\,\xi^2\kappa}\frac{10-3\,\xi^2\kappa}{12}\Bigg\}.\end{aligned} \tag{C11}$$

In the limit $\kappa \to 0$, Equation (C11) turns into

$$\lim_{\kappa\to 0}\frac{\lambda}{\lambda_{\rm M}} = \frac{23}{144\,\xi^7}. \tag{C12}$$

The result can be compared to Figure 5 for $\xi \in \{0.01, 0.05, 0.1\}$.

Many terms in the transport coefficients are of type $\kappa^{n/2}\,\mathcal{U}_{[l,m]}/\mathcal{U}_0$, which is

$$\chi \equiv \kappa^{n/2}\frac{\mathcal{U}\left(\frac{n+3}{2},\,\frac{n+5}{2}-\zeta,\,\kappa\,\xi^2\right)}{\mathcal{U}\left(\frac{3}{2},\,\frac{3}{2},\,\kappa\,\xi^2\right)}, \tag{C13}$$

where $l = (n+3)/2$ and $m = (n+5)/2 - \zeta$, for which the limit $\kappa \to 0$ can be estimated as follows. Considering $\kappa \ll 1$, if $\zeta = \kappa + 1 \approx 1$, then

$$\chi \approx \kappa^{n/2}\frac{\mathcal{U}\left(\frac{n+3}{2},\,\frac{n+3}{2},\,\kappa\,\xi^2\right)}{\mathcal{U}\left(\frac{3}{2},\,\frac{3}{2},\,\kappa\,\xi^2\right)} \tag{C14}$$

$$= \kappa^{n/2}\frac{\left(\frac{n-1}{2}-\kappa\,\xi^2\right)\Gamma\left(\frac{n-1}{2}\right)}{\Gamma\left(\frac{n+3}{2}\right)(\kappa\,\xi^2)^{(n+1)/2}} \times\frac{\Gamma\left(\frac{3}{2}\right)(\kappa\,\xi^2)^{1/2}}{\Gamma\left(\frac{1}{2}\right)+\Gamma\left(-\frac{1}{2}\right)\Gamma\left(\frac{3}{2}\right)(\kappa\,\xi^2)^{1/2}} \tag{C15}$$

$$= \frac{\left(\frac{n-1}{2}-\kappa\,\xi^2\right)\Gamma\left(\frac{n-1}{2}\right)}{\Gamma\left(\frac{n+3}{2}\right)\xi^n} \times\frac{\Gamma\left(\frac{3}{2}\right)}{\Gamma\left(\frac{1}{2}\right)+\Gamma\left(-\frac{1}{2}\right)\Gamma\left(\frac{3}{2}\right)(\kappa\,\xi^2)^{1/2}}, \tag{C16}$$

where we again made use of Equations (B12) and (B13). In the limit $\kappa \to 0$, we then obtain

$$\lim_{\kappa\to 0}\chi = \frac{\left(\frac{n-1}{2}\right)\Gamma\left(\frac{n-1}{2}\right)\Gamma\left(\frac{3}{2}\right)}{\Gamma\left(\frac{n+3}{2}\right)\xi^n\,\Gamma\left(\frac{1}{2}\right)} \tag{C17}$$

$$= \frac{1}{(n+1)\xi^n}. \tag{C18}$$

The case $\zeta = \kappa + 2 \approx 2$ yields

$$\chi \approx \kappa^{n/2}\frac{\mathcal{U}\left(\frac{n+3}{2},\,\frac{n+1}{2},\,\kappa\,\xi^2\right)}{\mathcal{U}\left(\frac{3}{2},\,\frac{3}{2},\,\kappa\,\xi^2\right)} \tag{C19}$$

$$= \kappa^{n/2}\frac{\left(\frac{n-3}{2}-\kappa\,\xi^2\right)\Gamma\left(\frac{n-3}{2}\right)}{\Gamma\left(\frac{n+3}{2}\right)(\kappa\,\xi^2)^{(n-1)/2}} \times\frac{\Gamma\left(\frac{3}{2}\right)(\kappa\,\xi^2)^{1/2}}{\Gamma\left(\frac{1}{2}\right)+\Gamma\left(-\frac{1}{2}\right)\Gamma\left(\frac{3}{2}\right)(\kappa\,\xi^2)^{1/2}} \tag{C20}$$

$$= \kappa\frac{\left(\frac{n-3}{2}-\kappa\,\xi^2\right)\Gamma\left(\frac{n-3}{2}\right)}{\Gamma\left(\frac{n+3}{2}\right)\xi^{2-n}} \times\frac{\Gamma\left(\frac{3}{2}\right)}{\Gamma\left(\frac{1}{2}\right)+\Gamma\left(-\frac{1}{2}\right)\Gamma\left(\frac{3}{2}\right)(\kappa\,\xi^2)^{1/2}}, \tag{C21}$$

Table 1
Overview of the Transport Coefficients

TC/Model	Maxwellian (M)	RKD	SKD	$\lim_{\kappa\to 0}$
Diffusion D	$\frac{4\sqrt{2}\,(k_B T)^{5/2}}{\pi^{3/2} m^{1/2} z e^4 L^{ei} n}$	$D_M \frac{\kappa^{5/2}\mathcal{U}_{[4,4]}}{\mathcal{U}_0}$	$D_M \frac{\Gamma(\kappa-3)}{\Gamma(\kappa-1/2)}\kappa^{5/2}$	$\frac{D_M}{6\xi^5}$
Mobility μ	$\frac{4\sqrt{2}\,(k_B T)^{3/2}}{\pi^{3/2} m^{1/2} z e^3 L^{ei} n}$	$\mu_M \frac{\kappa^{3/2}}{\mathcal{U}_0}[(\kappa+1)\mathcal{U}_{[4,3]} + \kappa\,\xi^2\,\mathcal{U}_{[4,4]}]$	$\mu_M \frac{\Gamma(\kappa-2)}{\Gamma(\kappa-1/2)}\kappa^{3/2}$	$\frac{\mu_M}{4\xi^3}$
Electric conductivity σ	$\frac{4\sqrt{2}\,(k_B T)^{3/2}}{m^{1/2}\pi^{3/2} z e^2 L^{ei}}$	$\sigma_M \frac{\kappa^{3/2}}{\mathcal{U}_0}[(\kappa+1)\mathcal{U}_{[4,3]} + \kappa\,\xi^2\,\mathcal{U}_{[4,4]}]$	$\sigma_M \frac{\Gamma(\kappa-2)}{\Gamma(\kappa-1/2)}\kappa^{3/2}$	$\frac{\sigma_M}{4\xi^3}$
Thermoelectric coefficient α	$-\frac{5}{2}\frac{k_B}{e}$	$\alpha_M \frac{\kappa\left[4(\kappa+1)\mathcal{U}_{[5,4]} - \frac{3}{2}\mathcal{U}_{[4,4]} + 4\kappa\,\xi^2\,\mathcal{U}_{[5,5]}\right]}{5/2[(\kappa+1)\mathcal{U}_{[4,3]} + \kappa\,\xi^2\,\mathcal{U}_{[4,4]}]}$	$\alpha_M \frac{\kappa}{\kappa-3}$	$\frac{2\,\alpha_M}{3\,\xi^2}$
Thermal conductivity λ	$\frac{16\sqrt{2}\,k_B (k_B T)^{5/2}}{m^{1/2}\pi^{3/2} z e^4 L^{ei}}$	$\lambda_M \frac{\kappa^{7/2}}{\mathcal{U}_0}[5(\kappa+1)\mathcal{U}_{[6,5]} + 5\,\xi^2\,\kappa\,\mathcal{U}_{[6,6]} - \frac{3}{2}\mathcal{U}_{[5,5]} - [(\kappa+1)\mathcal{U}_{[5,4]} + \xi^2\,\kappa\,\mathcal{U}_{[5,5]}]\frac{4(\kappa+1)\mathcal{U}_{[5,4]} - \frac{3}{2}\mathcal{U}_{[4,4]} + 4\kappa\,\xi^2\,\mathcal{U}_{[5,5]}}{(\kappa+1)\mathcal{U}_{[4,3]} + \kappa\,\xi^2\,\mathcal{U}_{[4,4]}}]$	$\lambda_M \frac{\Gamma(\kappa-4)}{\Gamma(\kappa-1/2)}\frac{\kappa^{7/2}(\kappa-1/2)}{(\kappa-3)}$	$\frac{23\,\lambda_M}{144\,\xi^7}$

Note. Displayed are the calculated transport coefficients ("TC"), i.e., diffusion coefficient D, mobility coefficient μ, electric conductivity σ, thermoelectric coefficient α, and thermal conductivity λ, based on different models, the Maxwellian (subscript M), the RKD (subscript RKD), and the SKD (subscript SKD). The last column shows the maximum values of the transport coefficients based on the $f_{r\kappa}$ in the limit $\kappa \to 0$ (and $\xi > 0$).

which in the limit $\kappa \to 0$ becomes

$$\lim_{\kappa \to 0} \chi = \kappa \frac{\left(\frac{n-3}{2}\right)\Gamma\left(\frac{n-3}{2}\right)\Gamma\left(\frac{3}{2}\right)}{\Gamma\left(\frac{n+3}{2}\right)\xi^{2-n}\,\Gamma\left(\frac{1}{2}\right)} \tag{C22}$$

$$= 0. \tag{C23}$$

Table 1 summarizes the results of this manuscript and contains the transport coefficients based on the Maxwellian distribution (subscript M), on the RKD and on the SKD. The last column shows the maximum values of the transport coefficients based on the RKD, obtained in the limit $\kappa \to 0$.

ORCID iDs

Edin Husidic https://orcid.org/0000-0002-1349-3663
Klaus Scherer https://orcid.org/0000-0002-9530-1396
Marian Lazar https://orcid.org/0000-0002-8508-5466
Horst Fichtner https://orcid.org/0000-0002-9151-5127
Stefaan Poedts https://orcid.org/0000-0002-1743-0651

References

Abramowitz, M., & Stegun, I. 1970, Handbook of Mathematical Functions (New York: Dover)
Balescu, R. 1988, Transport Processes in Plasmas—1. Classical Transport Theory (Amsterdam: North Holland Publishing Company)
Bhatnagar, P. L., Gross, E. P., & Krook, M. 1954, PhRv, 94, 511
Bian, N. H., Emslie, A. G., Stackhouse1, D. J., & Kontar, E. P. 2014, ApJ, 796, 142
Bourouaine, S., Marsch, E., & Neubauer, F. M. 2011, A&A, 536, A39
Boyd, T. J. M., & Sanderson, J. J. 2003, The Physics of Plasmas (Cambridge: Cambridge Univ. Press)
Braginskii, S. I. 1965, RvPP, 1, 205
Dum, C. T. 1990, in Physical Processes in Hot Cosmic Plasmas, ed. W. Brinkmann, A. C. Fabian, & F. Giovanelli (Dordrecht: Kluwer), 157
Ebne Abbasi, Z., Esfandyari-Kalejahi, A., & Khaledi, P. 2017, Ap&SS, 362, 103
Echim, M. M., Lemaire, J., & Lie-Svendsen, Ø. 2011, SGeo, 32, 1
Goedbloed, H., Keppens, R., & Poedts, S. 2019, Magnetohydrodynamics of Laboratory and Astrophysical Plasmas (Cambridge: Cambridge Univ. Press),
Guo, R., & Du, J. 2019, PhyA, 523, 156
Helander, P., & Sigmar, D. J. 2005, Collisional Transport in Magnetized Plasmas (Cambridge: Cambridge Univ. Press)
Husidic, E., Lazar, M., Fichtner, H., & Poedts, S. 2021, A&A, 654, A99
Landi, E. 2007, ApJ, 663, 1363
Landi, E., & Cranmer, S. R. 2009, ApJ, 691, 794
Landi, S., Pantellini, F., & Matteini, L. 2010, in AIP Conf. Proc. 1216, Twelfth International Solar Wind Conference, ed. M. Maksimovic et al. (Melville, NY: AIP), 218
Landi, S., Pantellini, F., & Matteini, L. 2012, ApJ, 760, 143
Lazar, M., & Fichtner, H. 2021, Kappa Distributions: From Observational Evidences via Controversial Predictions to a Consistent Theory of Non-equilibrium Plasmas (Berlin: Springer)
Lazar, M., Fichtner, H., & Yoon, P. H. 2016, A&A, 589, A39
Lazar, M., Poedts, S., & Fichtner, H. 2015, A&A, 582, A124
Lazar, M., Scherer, K., Fichtner, H., & Pierrard, V. 2020, A&A, 634, A20
Maksimovic, M., Zouganelis, I., Chaufray, J. Y., et al. 2005, JGR, 110, A09104
Marsch, E. 1994, AdSpR, 14, 103
Marsch, E. 2006, LRSP, 3, 1
Olbert, S. 1968, in Physics of the Magnetosphere, ed. R. L. Carovillano, J. F. McClay, & H. R. Radoski, Vol. 10 (Dordrecht: Reidel), 641
Oldham, K., Myland, J., & Spanier, J. 2009, An Atlas of Functions (New York: Springer)
Pierrard, V., & Lazar, M. 2010, SoPh, 267, 153
Salem, C., Hubert, D., Lacombe, C., et al. 2003, ApJ, 585, 1147
Scherer, K., Fichtner, H., Fahr, H. J., & Lazar, M. 2019, ApJ, 881, 93
Scherer, K., Fichtner, H., & Lazar, M. 2017, EL, 120, 50002
Scherer, K., Husidic, E., Lazar, M., & Fichtner, H. 2020, MNRAS, 497, 1738
Spatschek, K. H. 1990, Theoretische Plasmaphysik—Eine Einführung (Stuttgart: B.G. Teubner Verlag)
Vasyliūnas, V. M. 1968, JGRA, 73, 2839
Verscharen, D., Klein, K. G., & Maruca, B. A. 2019, LRSP, 16, 5
Vocks, C., & Mann, G. 2003, ApJ, 593, 1134
Vocks, C., Mann, G., & Rausche, G. 2008, A&A, 480, 527
Wang, L., & Du, J. 2017, PhPl, 24, 102305
Yoon, P. H. 2011, PhPl, 18, 122303
Yoon, P. H. 2014, JGRA, 119, 7074
Zouganelis, I., Meyer-Vernet, N., Landl, S., Maksimovic, M., & Pantellini, F. 2005, ApJL, 626, L117